JMEPEG (2007) 16:248–253
DOI: 10.1007/s11665-007-9045-z

1059-9495/$19.00

Tensile and Plane Bending Fatigue Properties of Two TRIP Steels at Room Temperature in the Air—A Comparative Study

M.A. Islam, S. Chen, and Y. Tomota

(Submitted April 20, 2006; in revised form May 11, 2006)

Due to worldwide environmental concerns, automobile industries are trying to reduce the weight of the vehicles without compromising the crashworthiness by employing high-strength steel sheets as much as possible. Transformation-induced plasticity (TRIP) steels, relatively newer in the structural application, might play an important role in this regard. In this present work, tensile and plane bending fatigue properties and fracture behaviors of two low-alloy TRIP (TRIP590 and TRIP780 grades) steels were investigated at room temperature in air. After mechanical tests, fractographic observations were carried out in the SEM. Both steels showed reasonably high values of elongations and fatigue limits. However, with an increase in the bending stress level, the fatigue performance of TRIP780 steel improved gradually.

Keywords ductile fracture, fatigue fracture, fatigue life, plane bending, tensile strength, TRIP steel

1. Introduction

The use of high-strength steels with excellent formability becomes a primary objective for economical, safety, and environmental reasons. Transformation-induced plasticity (TRIP) steels having high strength and excellent formability can answer the demand for weight reduction in auto bodies (Ref 1). Their excellent mechanical properties result from the martensitic transformation of metastable retained austenite (RA), induced by mechanical loading. The TRIP steels possess a multi-phase microstructure, consisting typically of ferrite, bainite, and retained austenite. The microstructure is obtained after intercritical annealing and subsequent isothermal annealing in the bainitic transformation region, called austempering. The carbon content in austenite is increased both during the intercritical annealing and the austempering. The carbon enrichment during austempering is the result of the suppression of the formation of carbides during the bainitic transformation, due to the presence of alloying elements such as Si and Al. The enrichment of C in the austenite increases its thermal as well as mechanical stability, and consequently, the austenite can be retained upon cooling to room temperature. This retained austenite then transforms to martensite due to high applied stress during forming, under service and in the event of a crash (Ref 1-4). The hard martensite delays the onset of necking resulting in a high total elongation, excellent formability, and high-energy absorption in the event of a crash enhancing the safety of passengers. In this work, initiative has been taken to discuss the tensile and fatigue properties of two low-alloy TRIP steels tested at room temperature in air.

M.A. Islam, S. Chen, and **Y. Tomota,** Institute of Applied Beam Science, Graduate School of Science and Engineering, Ibaraki University, 4-12-1 Nakanarusawa, Hitachi, Ibaraki 316-5226, Japan. Contact e-mail: urzsai@gmail.com.

2. Experimental

The materials of this study were commercially available TRIP steels having the chemical compositions presented in Table 1. Following necessary steps, metallographic samples were cut and mechanically polished on SiC papers and finally they were polished using gamma-alumina powder of 0.05 μm grain size. These specimens were then etched in 5% nital for few seconds to reveal the microstructures. After etching, they were observed in the scanning electron microscope (SEM) and photographed.

Tensile test was conducted on an Instron tensile testing machine at room temperature in air at a strain rate of 1.3×10^{-2}/s. The geometry of the test specimen is shown in Fig. 1. Figure 2 shows the geometry of the fatigue specimen. During fatigue testing, a negative strain ratio (R_e) of 1.0 (fully reversed) was used. The tests were carried out at a fixed-frequency of around 1000 cpm using a sinusoidal strain pattern of constant amplitude.

The bending moment (M_b) corresponding to the required level of applied stress was calculated using the following formula:

$$M_b = Z\sigma, \quad \text{(Eq 1)}$$

where Z is the coefficient of the cross section of the tested part and σ is the repeated bending stress in N/mm^2. The value of Z can be calculated from the following relationship:

$$Z = \frac{bh^2}{6}, \quad \text{(Eq 2)}$$

where b and h, respectively, are width and thickness of the specimen in millimeter. *Note*: For both tests, specimens were prepared in the direction of rolling.

After tensile and fatigue tests, specimens were cut behind the fracture surfaces to provide samples suitable for the SEM. The fracture surfaces of all specimens were then carefully observed and photographed in the SEM. The amount of retained austenite in the TRIP steels was measured by x-ray diffractometry (MO3XHF22, Mac Science Co., Ltd.) before and after fatigue fracture at different applied bending stress levels. In the x-ray analysis, a CrK_{α} source was used and the volume fraction of austenite was measured directly using the X-ray Powder Research Software System developed by Oxford Mac Science Co., Ltd.

3. Results

3.1 Microstructure

The TRIP steels usually possess a multi-phase microstructure, typically consisting of ferrite, bainite, and retained austenite. The microstructures of the steels used in present investigation are shown in Fig. 3. In 780 steel, there were some isolated martensite needles, and after tensile testing, the volume fraction of this phase increased (Fig. 3c). As per ASTM, the average ferrite sizes of steels A and B were 7 and 3 μm, respectively. It has been mentioned that RA (black region) in TRIP steels can remain as plate and blocky forms depending on the involved thermomechanical processes and resulting grain sizes (Fig. 4) (Ref 5).

Table 1 Chemical compositions of the steels (mass %)

Steels	C	Si	Mn	P	S	N
TRIP590	0.09	1.29	1.58	0.010	0.0014	0.005
TRIP780	0.19	1.21	1.60	0.008	0.0009	0.003

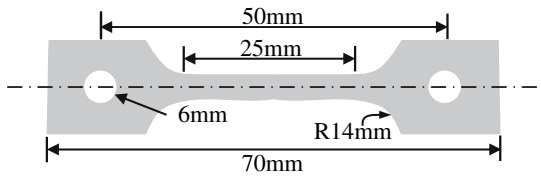

Fig. 1 Geometry of tensile test specimen

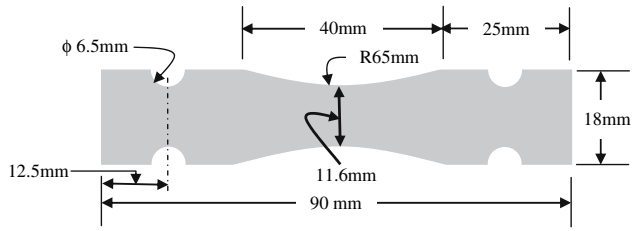

Fig. 2 Geometry of fatigue test specimen

3.2 Tensile Properties

The materials used in this experiment were low-alloy TRIP steels. The nominal stress-strain curves are shown in Fig. 5 and details of the tensile properties of these steels are presented in Table 2. From Fig. 5, it is evident that 590 steel showed discontinuous deformation with just a click indicating the yield point, whereas 780 steel exhibited continuous deformation without the indication of yield phenomenon. 780 steel gave comparatively lower elongation before final fracture. However, both steels showed reasonably high values of total elongation.

3.3 Fatigue Properties

The bending stress vs. number of cycles to failure curves, the S-N_f curves of the steels studied in the present work, are shown in Fig. 6. From these curves, it is clear that as the maximum stress values decrease the fatigue lives of the steels increase. Fatigue limit of 590 steel is at about 51% of the tensile strength and 84% of the yield strength. For 780 steel, it is at about 42% of tensile strength and 81% of the yield strength. The fatigue performance of 780 steel was better at any applied stress level and this was found to be further improved gradually with increasing load (Fig. 6).

3.4 Fractographic Observations

3.4.1 Fracture Surface of Tensile Specimens. The tensile fracture features of the steels observed under SEM reveal that the fracture morphologies were ductile microvoid coalescence. Nucleating on either inclusions or carbide particles, microvoids coalesce made larger dimples (Fig. 7). Although microvoid coalescence-type ductile fractures were observed on both steels, their fracture morphologies were somewhat different. 590 steel exhibited slightly larger dimples and in some regions of the fracture surface of 780 steel many microvoids were seen.

3.4.2 Fracture Surface of Fatigue Specimens. In both steels, the fracture nucleation sites were found on inclusions located at the surface and/or subsurface. Nucleating from one site, the crack propagated gradually inside the materials. For both steels, the crack formation and propagation patterns were almost

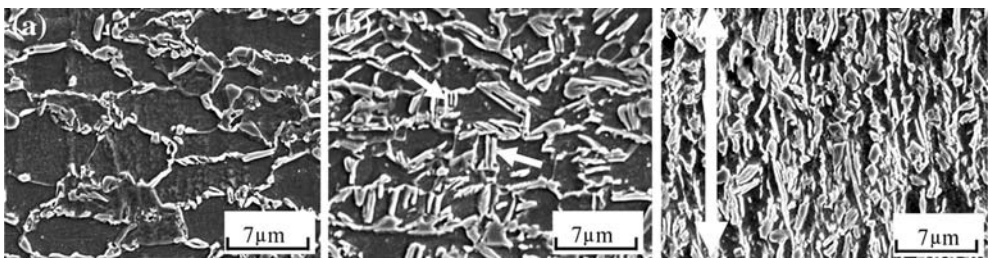

Fig. 3 Microstructures of (**a**) 590 and (**b**) 780 steels and (**c**) 780 steel after tensile test. Arrows on (**b**) are indicating the martensite needles and on (**c**) the direction of tensile loading

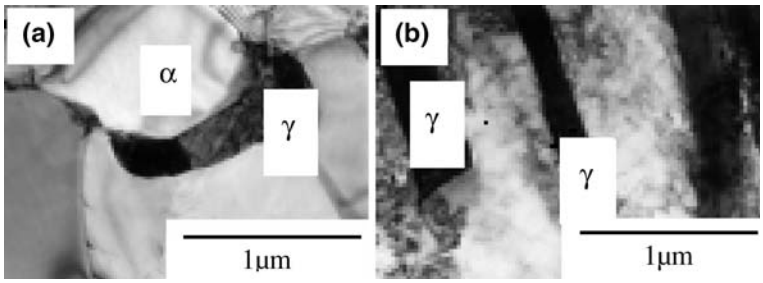

Fig. 4 TEM micrographs of the TRIP steels (**a**) fine grained and (b) coarse grained (after Ref 5)

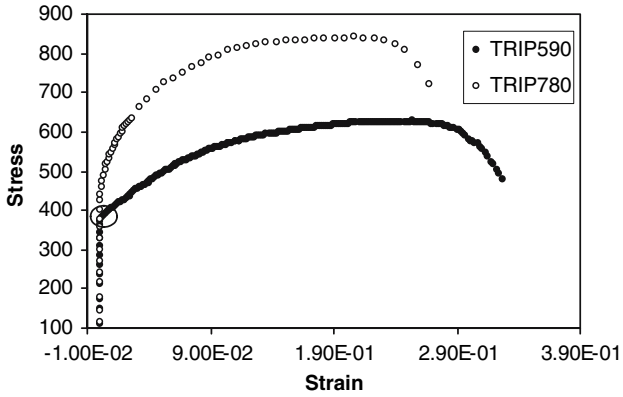

Fig. 5 Nominal stress-strain curves

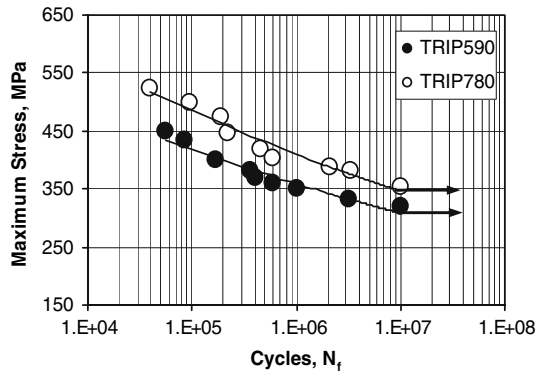

Fig. 6 *S*-N_f curves of the steels

the same (Fig. 8). Both steels showed almost completely transgranular quasi-cleavage fracture (Fig. 9). On the fracture surfaces of 590 steel, striation marks were found on transgranular facets and intergranular fracture was found on some isolated coarse-grained ferrites, however, for 780 steel such features were not observed (Fig. 10 and 11).

3.5 X-ray Diffractometry Results

X-ray diffraction was carried out to determine the amount of retained austenite in the steels. According to x-ray analysis, before fatigue testing, the volume fraction of retained austenite in 590 and 780 steels was 7.1 and 9.4%, respectively. For both steels, the proportions of retained austenite were found to decrease gradually with applied bending stress levels (Table 3).

4. Discussion

4.1 Tensile Properties

The mechanical properties especially tensile and fatigue are very much related to each other. It is a very common observation that the increase in the strain rate increases the yield and ultimate tensile strengths, which ultimately affect the fatigue life. In the present study, this has also been observed. The nominal stress-strain curves obtained from tensile tests are shown in Fig. 5. From this figure, it is clear that the 590 steel, at the yield stress level, exhibited a sudden increase in the strain in relation to the applied stress, whereas 780 steel showed no yield point. Continuous yielding is considered due to the large amount of martensite, whereas the yield point phenomena, i.e., discontinuous yielding, are observed in the low-carbon steels containing a higher proportion of ferrite (Ref 6, 7). In-situ neutron diffraction revealed that carbon-enriched austenite is plastically harder than the ferrite matrix and this phase plays an important role in continuous deformation during early stage of deformation (Ref 3). In the present study, 590 steel has the carbon content lower than 780 steel. Plausibly, the carbon content in the retained austenite in 780 steel is higher than that

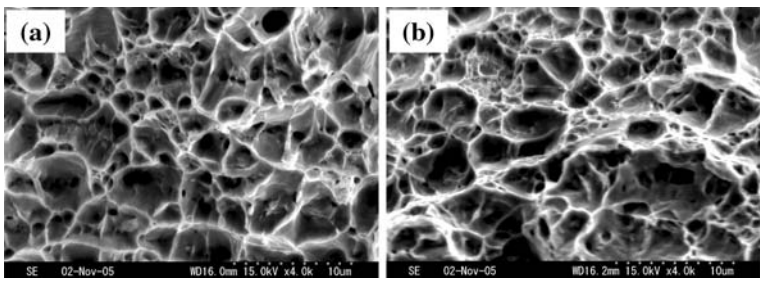

Fig. 7 Ductile fracture on tensile specimens (**a**) 590 and (**b**) 780 steels

Table 2 Tensile properties of the steel

Steels	YS, MPa	UTS, MPa	Total EL%
TRIP590	380	626	32.7
TRIP780	441	840	26.8

of 590 steel. Moreover, the volume fraction of relatively harder retained austenite in 780 steel is also higher. Due to all these factors, 780 steel showed continuous deformation from the early stage. In the later stages, stress-induced transformation of RA to martensite takes place and this happens continuously with deformation (Ref 3, 7, 8). So, the enhancement of uniform elongation in both steels in the later stage is caused by the second phase hardening not by the transformation strains. The internal stress yielded by the plastic misfit strain increases the work hardening rate resulting in delay of microscopic necking, and hence, a high-uniform elongation is achieved. The presence of the higher proportion of martensite needles seen in Fig. 3c also suggests martensite formation under stress. The total elongation of 780 steel is lower than that of 590 steel. This is due to higher carbon and lower-grain size that made the average hardness and strength of the steel significantly higher.

4.2 Fatigue Properties

From the S-N_f curves (Fig. 6), it is clear that as the applied bending stress decreased the corresponding number of cycles to failure increased for both steels. However, compared to 590 steel, 780 steel has better fatigue performance at any stress level, which is also found to improve gradually with the increase in the bending stress levels. The better fatigue performance of 780 steel can be explained by the higher tensile and yield strengths, which control the fatigue crack nucleation in the materials. It has been mentioned that austenite containing higher carbon is plastically harder and more stable (Ref 3, 6, 9, 10). During the fatigue test, stress-induced phase transformation of austenite to martensite takes place. Usually the stress required to initiate this sort of phase transformation depends on the martensite transformation start temperature (M_S temperature) of the steel (Ref 11). At higher temperatures, the retained austenite still transforms to martensite, however, depending on the temperature, progressively higher stresses will be needed. Moreover, higher-carbon content makes the retained austenite more mechanically and thermally stable (Ref 9). In the present study, the carbon content of 780 steel is double of that in the 590 steel, which made the RA in the former more stable. To initiate transformation of RA to martensite, 780 steel needs a comparatively higher-stress level. As a result, the transformation-induced local strengthening effect in 780 steel at lower stress levels is less pronounced than that in the 580 steel, which is clear from Table 3. From Fig. 4, it is revealed that RA could be present in the steel as plate and blocky forms depending on the grain size. Compared to plate-like RA, blocky RA can relax the induced stress more readily during deformation. Due to the stress concentration effect, the local stress on plate-type RA above the critical level of stress can transform the RA to martensite, although the gross applied stress levels were apparently lower. This situation might help to transform a certain proportion of retained austenite to martensite in both steels at lower applied stress levels.

4.3 Fractographic Observation

4.3.1 Tensile Fracture Surfaces. The main observations on tensile fracture surfaces were that both steels showed microvoid coalescence-type ductile fracture with small voids slightly more evident in the latter (Fig. 7). During tensile loading of any specimen, crack initiation occurred at the centre by fracturing the inclusion/matrix interfaces or from a pre-existing microcrack at the interface (e.g., MnS inclusion/matrix interface) at the grain boundaries, and/or within the grains. The microcrack produces a triaxial stress state in the specimen, which promotes void nucleation and growth around the larger particles. Further strain causes these voids to coalesce. At some point, the deformation and longitudinal crack growth cannot continue when the work hardening capacity is exhausted and final failure takes place.

The tensile fracture surfaces at room temperature are composed of microvoid coalescence-type fractures. Since 590 steel has coarser and softer ferrite grain sizes, the spacing

Table 3 Variations of RA with bending stress (BS, MPa) levels

TRIP590 steel				TRIP780 steel			
BS	N_f	% RA	% Transformation	BS	N_f	% RA	% Transformation
0	0	7.1(±0.5)	...	0	0	9.4(±1.2)	...
433	85,600	4.3(±0.23)	40	500	96,000	4.4(±0.16)	53

Note: locations 2 mm from the fracture surfaces were analyzed

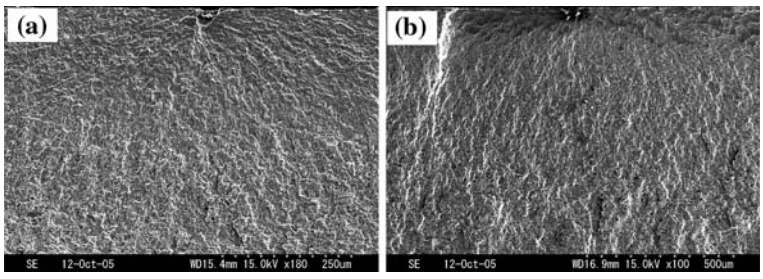

Fig. 8 SEM micrographs showing the fatigue crack nucleating sites (**a**) 590 and (**b**) 780 steels

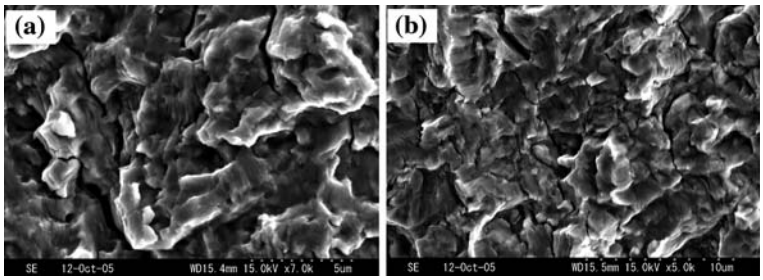

Fig. 9 Transgranular quasi-cleavage fractures (**a**) 590 and (**b**) 780 steels

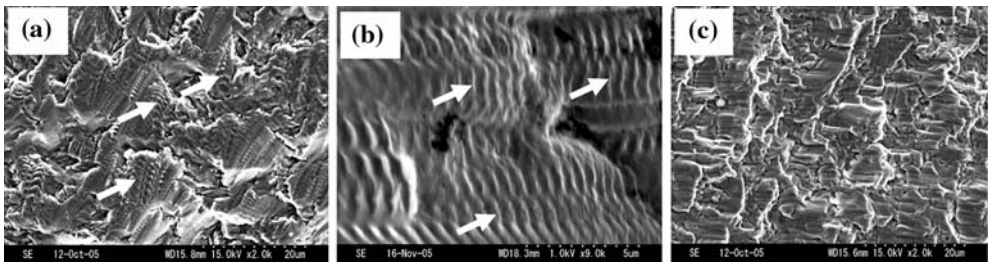

Fig. 10 (**a**) Striation marks (marked by arrows) on some isolated areas of 590 steel, (**b**) close-up view of the striation marks indicated by arrows, and (**c**) fracture surface on 780 steel at the same level of crack length of (**a**)

between crack nucleating inclusions (i.e., inclusions between one grain boundary and another) is arguably higher. As a result, an individual microvoid needs to grow to a greater extent to join with adjacent voids. This overall process makes the ductile voids in 590 steel seem somewhat coarser, which can be distinguished under close observation. The concentration of strain provides sufficient plasticity to nucleate voids around smaller, but more numerous, particles (e.g., carbide particles). These smaller particles are usually very closely spaced. As both steels have a similar chemical composition except for C, which is more than doubled in the 780 steels, carbide particle-induced microvoids are more evident in 780 steel.

4.3.2 Fatigue Fracture Surfaces. In these steels, crack nucleation sites were found on inclusion particles (Fig. 8). This is because the critical stress required to nucleate the fatigue crack is lowered at microscopically weak areas. On the tensile fracture some microvoids, especially on 780 steel, seemed to nucleate from fine carbide particles. However, carbide nucleated fatigue cracks were not observed. The possible reason for this is that inclusions are coarser, which also cause microscopically greater weakness. So, they are more potent in nucleating a fatigue crack. Moreover, in the case of uniaxial tension, cracks are formed on inclusion particles and they grow with strain. The concentration of strain provides sufficient plasticity to nucleate voids around relatively smaller carbide particles. However, this micromechanism of crack formation is not active in the case of plane bending fatigue.

From Fig. 9, it is clear that the fatigue fracture mode is completely transgranular for both steels. The brittle fracture in steel is usually transgranular quasi-cleavage, because the cohesive strength of the transgranular cleavage plane is lower than the intergranular cohesive strength (if there is no significant grain boundary weakening due to impurity element segregation or carbide precipitation), and the cracks propagate

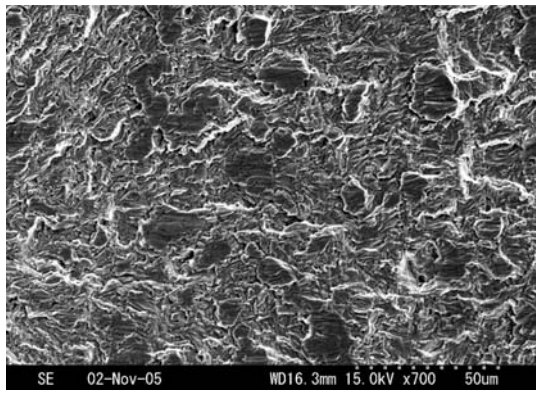

Fig. 11 Intergranular fracture on 590 steel tested at low stress level

preferentially along weaker paths. As fatigue fracture is a brittle type of fracture, the transgranular fatigue fracture morphologies of these steels are quite usual. Fatigue cracks grow with the number of cycles making striations. The striations are only visible on some isolated transgranular facets of 590 steel. This phenomenon can be explained by the fact that this steel has relatively coarser and softer ferrites. Moreover, some isolated ferrite grains were found to be significantly coarser than the average grain size of this steel and formation of striations on the isolated coarse-grained ferrite was easier. For a very low bending stress, the 590 steel exhibited some isolated intergranular fractures (Fig. 11). This figure revealed that most of the intergranular facets are near the coarse ferrite grain boundaries. As the grain size increases, the grain boundary cohesive strength gradually deceases due to trace element segregation and/or heavier carbide particle precipitation. Moreover, the fatigue test was carried out at room temperature in air, which

may also cause environmental interaction to reduce the grain boundary strength and encourage intergranular fracture.

5. Conclusions

1. Metallographic observation revealed the microstructures of the steels to be composed of ferrite, bainite, and retained austenite. However, 780 steel exhibited few martensite-like needles with the other phases. After tensile and fatigue tests, the volume fraction of martensite increased.
2. Both steels exhibited ductile microvoid coalescence-type fracture under tensile loading and brittle transgranular fracture under fatigue loading at room temperature in air.
3. Although the RA content in 780 steel was significantly higher than in 590 steel, the latter showed better ductility, suggesting that RA cannot control the ductility of the TRIP steel. The 780 steel showed significantly higher strength without a significant decrease in ductility. This steel also exhibited better fatigue life, which improved further at higher stress level.

Acknowledgments

The authors acknowledge Dr. S. Nishino of Institute of Applied Beam Science, Ibaraki University for providing the steels and members of Professor Y. Tomota research group for their cooperation during various stages of this research. One of the authors (MAI) is also grateful to the JSPS authority for supporting him during the tenure of this research work.

References

1. M. Takahashi, O. Kawano, T. Hayashida, R. Okamoto, and H. Taniguchi, High Strength Hot-Rolled Steel Sheets for Automobiles, Nippon Steel Technical Report No. 88, July 2003, p 1–12
2. D. Beynon, T.B. Jones, and G. Fourlaris, Effect of High Strain Rate Deformation on Microstructure of Trip Steels Tested Under Dynamic Tensile Conditions, *Mater. Sci. Technol.*, 2005, **21**(1), p 103–112
3. Y. Tomota, H. Tokuda, Y. Adachi, M. Wakita, N. Minakawa, A. Moriai, and Y. Morii, Tensile Behavior of TRIP-Aided Multiphase Steels Studied by In situ Neutron Diffraction, *Acta Mater.* 2004, **52**, p 5737–5745
4. K. Hulka, The Role of Niobium in Cold Rolled Trip Steel, *J. Mater. Sci. Forum*, 2005, **473**, p 91–102
5. M. Wakida, Y. Adachi, S. Shimokawa, and Y. Tomota, Ultrafine TRIP-Aided Multi-phases Steels, *CAMP-ISIJ*, 2005, **18**, p 613
6. M.H. Saleh and R. Priestner, Retained Austenite in Dual-Phase Silicon Steels and Its Effect on Mechanical Properties, *J. Mater. Process. Technol.*, Elsevier Science Ltd, 2001, **113**, p 587–593
7. S-J. Kim, C.G. Lee, T-H. Lee, and C-S. Oh, Effect of Cu, Cr and Ni on Mechanical Properties of 0.15 wt.% C TRIP-Aided Cold Rolled steels, *J. Scripta Mater.*, 2003, **48**, p 539–544
8. E. Girault, A. Mertens, P. Jacues, Y. Houbaert, B. Verlinden, and J.V. Humbeeck, Comparison of the Effects of Silicon and Aluminium on the Tensile Behavior of Multiphase TRIP-Assisted Steels, *J. Scripta Mater.*, 2001, **44**, p 885–892
9. S. Zaefferer, J. Ohlert, and W. Bleck, A Study of Microstructure, Transformation Mechanisms and Correlation Between Microstructure and Mechanical Properties of a Low Alloyed TRIP Steel, *J. Acta Mater.*, Elsevier Science Ltd, 2004, **52**, p 2765–2778
10. D. Son, H. Choi, and E. Shin, Analysis of the retained austenite stability in TRIP steels by X-ray and Neutron diffraction, *Proc. of the International Symposium on Research Reactor and Neutron Science—In Commemoration of the 10th Anniversary of HANARO*—Daejeon, Korea, April 2005, p 706–710
11. B.C.D. Cooman, Structure-Property Relationship in TRIP Steels Containing Carbide Free Bainite, *J. Solid State Mater. Sci.*, Elsevier Science Ltd, 2004, **8**, p 285–303